Article

Spontaneous resolution of chiral 3-(2,3-dimethylphenoxy)propane-1,2-diol under the circumstances of an unusual diversity of racemic crystalline modifications

Alexander A Bredikhin, Dmitry V. Zakharychev, Zemfira A. Bredikhina, Alexey V Kurenkov, Dmitry B. Krivolapov, and Aidar T. Gubaidullin

Cryst. Growth Des., **Just Accepted Manuscript** • DOI: 10.1021/acs.cgd.7b00510 • Publication Date (Web): 10 Jul 2017

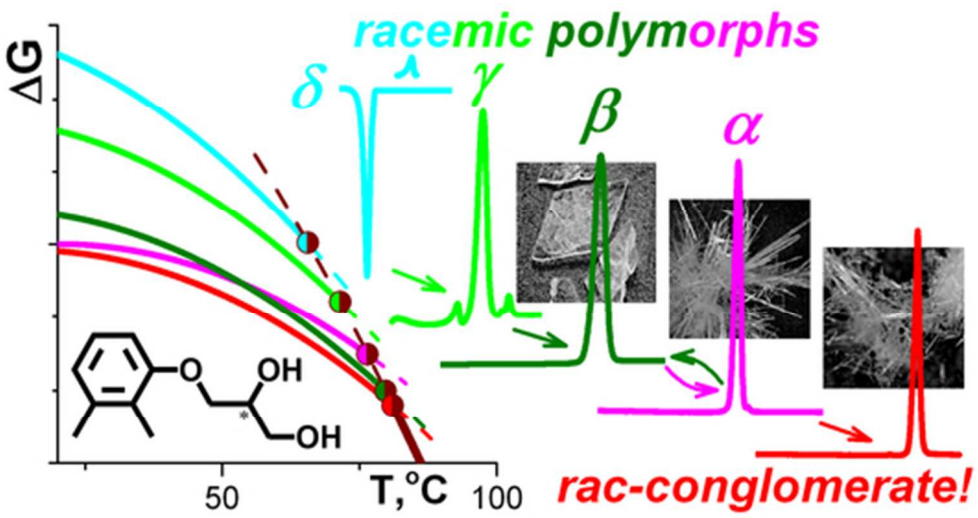

Graphical abstract

45x23mm (300 x 300 DPI)

Cover Page

Spontaneous resolution of chiral 3-(2,3-dimethylphenoxy)propane-1,2-diol under the circumstances of an unusual diversity of racemic crystalline modifications

Alexander A. Bredikhin*, Dmitry V. Zakharychev, Zemfira A. Bredikhina, Alexey V. Kurenkov, Dmitry B. Krivolapov, Aidar T. Gubaidullin

A.E. Arbuzov Institute of Organic and Physical Chemistry of Kazan Scientific Center of Russian Academy of Sciences, Arbuzov St., 8, Kazan 420088, Russian Federation

Chiral phenyl glycerol ether bearing two methyl groups in the *ortho* and *meta* positions, 3-(2,3-dimethylphenoxy)propane-1,2-diol **1**, crystallizes from the racemic feed medium with the formation of five crystalline modifications: *α-rac*, *β-rac*, *γ-rac*, *δ-rac* racemic compounds and racemic conglomerate. The *α-rac*, *β-rac* and racemic conglomerate are formed during solutions crystallization as good crystals, the nature of which was established by single crystal X-ray diffraction. The *γ-rac* and *δ-rac* are formed during *rac*-**1** crystallization from melt. The graphs of the dependence of free Gibbs energy on temperature were constructed. The *δ-rac* phase is unstable and turns into *γ-rac,* further the last spontaneously recrystallizes into *β-rac*. Stable in dry state, in a solvent medium *β-rac* is converted to *α-rac*. Crystallization of *rac*-**1** from solutions at room temperature leads to the *α-rac* phase which is stable both in dry form and in solutions. Taking into account that above room temperature the conglomerate is thermodynamically more favorable than all polymorphic racemic compounds, and that this particular form crystallizes from solutions under the condition of initial enantiomeric enrichment of the sample, we realized a successful direct resolution of *rac*-**1** into individual enantiomers.

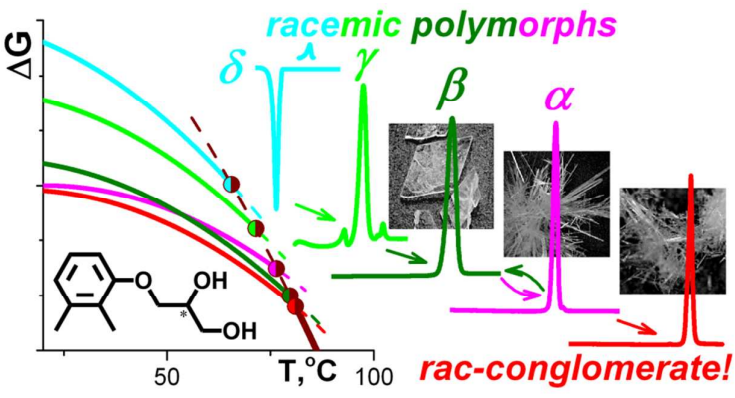

* Corresponding author: Phone/fax: +7 843 2727393/ +7 843 2731872. E-mail: baa@iopc.ru.

Spontaneous resolution of chiral 3-(2,3-dimethylphenoxy)propane-1,2-diol under the circumstances of an unusual diversity of racemic crystalline modifications

Alexander A. Bredikhin*, Dmitry V. Zakharychev, Zemfira A. Bredikhina, Alexey V. Kurenkov, Dmitry B. Krivolapov, Aidar T. Gubaidullin

A.E. Arbuzov Institute of Organic and Physical Chemistry of Kazan Scientific Center of Russian Academy of Sciences, Arbuzov St., 8, Kazan 420088, Russian Federation

ABSTRACT

Depending on the conditions of crystallization from solutions, racemic 3-(2,3-dimethylphenoxy) propane-1,2-diol **1** forms three relatively stable crystalline modifications. Each of the crystalline forms, namely, two polymorphic racemic compounds and a racemic conglomerate, have been characterized by single crystal XRD. Two more metastable racemic compounds crystallized from the racemic melt have been found by DSC method. Additional thermochemical investigations allowed to plot the dependence of the free Gibbs energy on temperature for all the phases found. With the help of slurrying experiments, the nature of the transitions between solid phases has been specified. It has been found that even a slight predominance of one of the enantiomers in almost racemic **1** samples ensures the crystallization of the conglomerate. The revealed features of *rac*-**1** crystallization have been taken into account during the realization of its resolution into individual enantiomers by the entrainment procedure.

INTRODUCTION

Polymorphism is an evergreen theme for researchers of molecular crystals.[1,2] Current interest in this problem is largely supported by the needs of pharmaceutical science and industry.[3,4] In recent years, chiral compounds are increasingly becoming objects of the research.[5-11] An additional feature of chiral systems that is absent in the case of achiral substances is the possible interconversion of homochiral (scalemic, enantiopure) and heterochiral (mainly racemic) crystalline forms.[12-14] In the strict sense of the word, conglomerate homochiral crystals are not polymorphic with respect to any racemic solid. However, like ordinary polymorphs, those and others can be formed from a common feed medium (solution or melt) and can transform into each other both as a result of solid-phase transitions and as a result of contact with the common

liquid phase.[12] Lack of attention to this feature of a phase behavior of the chiral substance can lead to withdrawal of the dosage form from the market and/or the need for remarketing of the already registered drug.[14 and references therein]

The object of the present work is 3-(2,3-dimethylphenoxy)propane-1,2-diol **1** (Chart 1), a glycerol phenyl ether bearing two methyl groups in the *ortho* and *meta* positions of the phenyl ring.

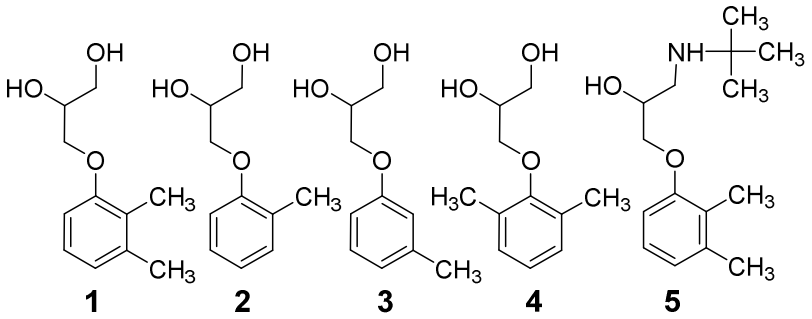

Chart 1. 3-(2,3-Dimethylphenoxy)propane-1,2-diol **1**
and some structurally related compounds mentioned in the text

By its chemical structure, it belongs to a series of chiral terminal aromatic glycerol ethers (TAGE) with the general formula Ar-O-$CH_2CH(OH)CH_2OH$, which possess a number of valuable and interesting properties for the researcher.[15] In particular, in this series there is an increased frequency of conglomerates,[16] the existence of polymorphic modifications has been proved for the racemic crystals.[9,11] Finally, in this series the unique of its kind solid-phase transition between the metastable anomalous and stable normal conglomerates has been observed.[9] We believe that the accumulation and systematization of information on the crystal structure, phase diversity, quantitative characteristics of solid phases and transitions between them in a series of structurally close compounds will broaden and deepen our understanding of the relationship between the chemical structure of matter and its properties.

We have previously shown that the mono *ortho* methyl-substituted phenyl glycerol ether **2** (Chart 1, API *mephenesin*) from the racemic feed material crystallizes as a normal conglomerate,[17] that is, it prones to spontaneous resolution during crystallization. Furthermore, the appearance of additional methyl group in the second *ortho* position of the benzene ring in the glycerol ether **4** changes dramatically its crystal structure in comparison with **2**, but does not change the type of crystallization, and this chiral diol remains a normal conglomerate.[18] At the same time, the racemic *meta*-substituted mephenesin analogue **3** crystallizes as a normal racemic compound.[17]

Judging from the literature, (*S*)-**1** (mp 104–105 ^{o}C)[19] melts 21 degrees above than *rac*-**1** (mp 82.5-83 ^{o}C).[20] In this connection, compound **1** could also be expected to crystallize in the form of

a conglomerate. As will be shown below, these expectations are to some extent justified, but the presence of a second methyl substituent leads to rather unexpected consequences.

Diol **1** shares a common part and can be used as a precursor for the synthesis of API *xibenolol* **5** (Chart 1). Xibenolol is the common name for 1-(*tert*-butylamino)-3-(2',3'-dimethylphenoxy)-2-propanol and is a selective β–adrenergic blocker.[21] Its salt, *xibenolol hydrochloride*, in racemic form is present at the market as the antiarrhythmic remedy under the trade names Selapin and Rhythminal. Therefore, the effective production of **1** in the scalemic (nonracemic, enantiopure) forms by stereoselective crystallization may not only be of theoretical but also of practical interest, since synthetic routes exist for converting this diol to single enantiomer forms of xibenolol.[19]

EXPERIMENTAL SECTION

Instrumentation. The IR spectra of the polycrystalline samples of *rac*- and (*R*)-diols **1** in KBr pellets were recorded on a Bruker Tensor 27 spectrometer. Optical rotations were measured on a Perkin–Elmer model 341 polarimeter (concentration *c* is given as grams per 100 milliliters). Melting points for general purposes were determined using a Boëtius apparatus. HPLC analyses were performed on a Shimadzu LC-20AD system controller, using UV detector. The thermograms were measured on a Netzsch DSC 204 F1 Phoenix differential scanning calorimeter (τ-sensor) in aluminum pans with the rate of heating and cooling of 5 ^{o}C min^{-1}. The mass of the samples amounted to about 1-5 mg for determining the characteristic temperatures of the processes and measuring the enthalpies of phase transitions, and 5-10 mg for measurements of heat capacities. The mass of the samples was controlled with Sartorius CPA 2P balance. The heat capacities were measured in continuous mode at a heating rate of 5 °C/min. The standard calibration of the instrument was performed using the temperatures and enthalpies of melting for In, Sn, and Bi standards and the phase transition in adamantane. Verification of calibration accuracy and measurement error estimation for temperature and enthalpy of melting values was carried out by melting samples of naphthalene and benzoic acid, and for heat capacity measurements by recording a thermogram of corundum disk (m = 50 mg). The reproducibility for the measured temperature values was ~ 0.3 ^{o}C, for the melting enthalpies better than 1%, and for the heat capacities ~ 2-5%.

Substances. Racemic and enantiopure 3-(2,3-dimethylphenoxy)propane-1,2-diol were prepared by analogy with published procedure.[18] A detailed description of the experiment and NMR spectra of the samples were given in the Supporting Information.

*rac-3-(2,3-Dimethylphenoxy)propane-1,2-diol, rac-**1.3**:* mp 81.5-90 ^{o}C (light petroleum ether/ EtOAc) [lit.[20] mp 82.5-83 ^{o}C (ligroin; benzene)].

*(R)-3-(2,3-Dimethylphenoxy)propane-1,2-diol, (R)-**1***: mp 101-102.5 °C (light petroleum ether/ EtOAc); $[\alpha]_D^{20}$ = +1.4 (*c* 1.0, EtOH), $[\alpha]_D^{20}$ = +13.4 (*c* 1.1, MTBE), {lit.[22] $[\alpha]_D^{25}$ = +1.44 (*c* 1.0, EtOH) 96.6 % *ee*}; 99.3% *ee* [chiral HPLC analysis; Daicel Chiralcel OD (0.46 x 25 cm) column; eluent hexane/isopropanol = 8:2; flow rate 1.0 mL/min; UV detector 275 nm (t_R = 11.2 min)].

*(S)-3-(2,3-Dimethylphenoxy)propane-1,2-diol (S)-**1**:* mp 101.5-103 °C; $[\alpha]_D^{20}$ = –1.0 (*c* 1.1, EtOH), $[\alpha]_D^{20}$ = –13.5 (*c* 1.0, MTBE), $[\alpha]_D^{20}$ = +2.3 (*c* 1.1, $CHCl_3$) {lit.[19] mp 104–105 °C (EtOH); $[\alpha]_D^{25}$ = +4.25 (c 1.0, $CHCl_3$)}; 99.9 % *ee* (chiral HPLC analysis; t_R = 13.0 min).

Solubility and nucleation boarder studies. In order to determine the solubility, the polythermal laser monitoring last crystal disappearance method was used. Precisely controlled samples [Shimadzu AUW 120D analytic balance (accuracy ± 0.01 mg)] of *rac*-**1** and (*S*)-**1** in 1 ml of solvent were placed in sealed glass vial, equipped with magnetic stir bar. For precise temperature control another vessel equipped with a controlling thermometer, a stir bar and a solvent was placed just near the test vial. All the vessels were placed in a thermostatic container. The suspension of the sample was agitated at about 400 rpm, increasing the temperature gradually (0.5 °C/min). The turbidity degree was registered to detect the "clear point". The temperature where the last crystals disappeared was taken as saturation temperature. After complete dissolution of the crystals in the studied reactor the coolant was slowly cooled down (0.3 °C/min), detecting the so-called 'cloud points' (the temperature where the first crystals were reliably detected) in cooling cycles. Each "heating-cooling" cycle was repeated three times. As the limits of the range, the lowest value of the recorded end-of-dissolution temperature and the highest value of the crystallization start temperature were selected.

Racemic 3-(2,3-dimethylphenoxy)propane-1,2-diol, *rac*-1 resolution by entrainment. Racemic diol *rac*-**1** (1.350 g) and (*R*)-**1** (0.150 g) was dissolved in 176.5 ml of water at 50 °C. The solution was cooled to 39 °C and then seeded with finely pulverized (*R*)-**1** (0.008 g). After stirring the mixture for 107 min at 37.5 °C, precipitated (*R*)-**1** was collected by filtration (0.295 g after drying; 87.4 % *ee*). The extra portion of *rac*-**1** (0.287 g) was then dissolved in the mother liquor at 50 °C. The resulting solution was cooled to 39 °C. After the addition of (*S*)-**1** (0.008 g) as seed crystals to the solution, and stirring the mixture for 90 min at 37.5 °C, (*S*)-**1** (0.320 g after drying; 53.2 % *ee*) was collected by filtration.

X-ray Analysis. The crystals of *rac*-**1**.**1** (prisms, mp 79.5-82 °C) and *rac*-**1**.**2** (needles, mp 76.5-78 °C) for single crystal X-ray diffraction analysis were prepared by slow evaporation of the solution of racemic sample in a mixture of cyclohexane and EtOAc at ambient temperature. A single crystal, selected at random from the racemic polycrystalline sample *rac*-**1**.**3**, which was prepared by rapid recrystallization of the racemic sample from the hot solution in a light

petroleum ether and EtOAc mixture, was used for X-ray analysis; this crystal was designated also as *S*-**1**.

The X-ray diffraction data for these crystals were collected on a Bruker AXS Smart Apex II CCD diffractometer in the ω-scan and φ-scan modes using graphite monochromated Mo Kα (λ 0.71073 Å) radiation at 296(2) K. The crystal data, data collection, and the refinement parameters are given in Table 1.

Data were corrected for the absorption effect using SADABS program.[23] The structures were solved by direct method and refined by the full matrix least-squares using SHELX[24] and WinGX[25] programs. All non-hydrogen atoms were refined anisotropically. All hydrogen atoms were inserted at calculated positions and refined as riding atoms except the hydrogen atoms of OH groups which were located from difference maps and refined isotropically or as riding atoms. All figures were made using Mercury program.[26] Molecular structures and conformations were analyzed by PLATON.[27]

Crystallographic data for the structures *rac*-**1.1,** *rac*-**1.2** and *rac*-**1.3** reported in this paper were deposited with the Cambridge Crystallographic Data Centre as supplementary publication number CCDC 1538660 – 1538662 respectively. Copies of the data can be obtained, free of charge, on application to CCDC, 12 Union Road, Cambridge CB2 1EZ, UK, (fax: +44-(0)1223-336033 or e-mail: deposit@ccdc.cam.ac.uk).

Table 1
Crystallographic data for crystals picked from *rac*-1.1, *rac*-1.2, and *rac*-1.3 samples

compound	***rac*-1.1**	*rac*-**1.2**	***rac*-1.3 (*S*-1)**
sample formula		C11 H16 O3	
M (g/mol)		196.24	
temperature, K	296(2)	296(2)	296(2)
crystal class	Monoclinic	triclinic	monoclinic
space group	$C2/c$	$P\bar{1}$	$P2_1$
crystal size	0.50x0.50x0.2 mm^3	0.4x0.01x0.01	0.36x0.10x0.10
Z, Z′	8, 1	2,1	4, 2
cell parameters	a = 37.05(2) Å, b = 5.859(4) Å, c = 9.685(6) Å 102.786(8)°	4.808(3) 5.858(3) 18.302(10) 94.501(7) 93.993(8) 91.813(7)	12.831(16) 5.037(6) 17.50(2) 101.813(15)
V ($Å^3$)	2050(2)	512.3(5)	1107(2)
F(000)	848	212	424
ρ_{calcd} (g/cm^3)	1.271	1.272	1.177
μ (cm^{-1})	0.91	0.91	0.85
θ (deg)	2.255-29.504	2.238-29.476	1.621-29.329
reflns measured	12157	6293	9632
independent reflns / R(int)	2702 / 0.0334	2570/0.0350	4939/0.1152
Number of params / restraints	137 / 0	135/2	262/1
Reflns [$I > 2\sigma(I)$]	1866	1450	1472
R_1 / wR_2 [$I > 2\sigma(I)$]	0.0437 / 0.1155	0.0542/0.1459	0.0834/0.1605
R_1 / wR_2 (all reflns)	0.0674 / 0.1311	0.1045/0.1708	0.2751/0.2376
GOF on F^2	0.985	1.034	0.877
ρ_{max}/ρ_{min} (e $Å^{-3}$)	0.189 / -0.153	0.182 / -0.162	0.185 / -0.212

RESULTS AND DISCUSSION

Synthesis of 3-(2,3-dimethylphenoxy)propane-1,2-diol and diversity of its crystal forms. The samples of racemic diol **1** required for the initial study were obtained by the interaction of 2,3-dimethylphenol with racemic 3-chloropropane-1,2-diol.

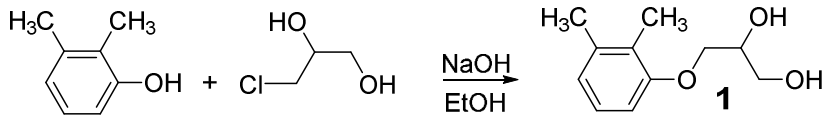

To obtain the scalemic diols we have used commercially available single enantiomeric (*R*)- and (*S*)-3-chloropropane-1,2-diols (see ESI for details).

Slow room temperature evaporation of solutions of racemic diol **1** in a mixture of cyclohexane and a small amount of ethyl acetate leads to the formation of two types of crystals on the bottom of the vessel: flat transparent prisms (Figure 1a, we will denote such samples as *rac*-**1**.**1**) and characteristic beams of crystals forming around the common center (Figure 1b, *rac*-**1**.**2**). Rapid cooling of heated concentrated solutions of racemic **1** in a mixture of light petroleum and ethyl acetate results in the formation of loose polycrystalline samples in which the crystals retain the acicular habitus (Figure 1c; hereinafter the appropriate crystalline samples will be referred to as *rac*-**1**.**3**). The *rac*-**1**.**3** samples melt over a wide temperature range of 81.5-90 °C, which is typical for conglomerate-forming compounds. Crystallization of *scal*-**1** from a mixture light petroleum/EtOAc leads to needles that differ markedly in size within the same sample (Figure 1d). In their appearance, they resemble *rac*-**1**.**3** crystals. The scalemic crystals melt in a narrow range of 101-102.5 °C.

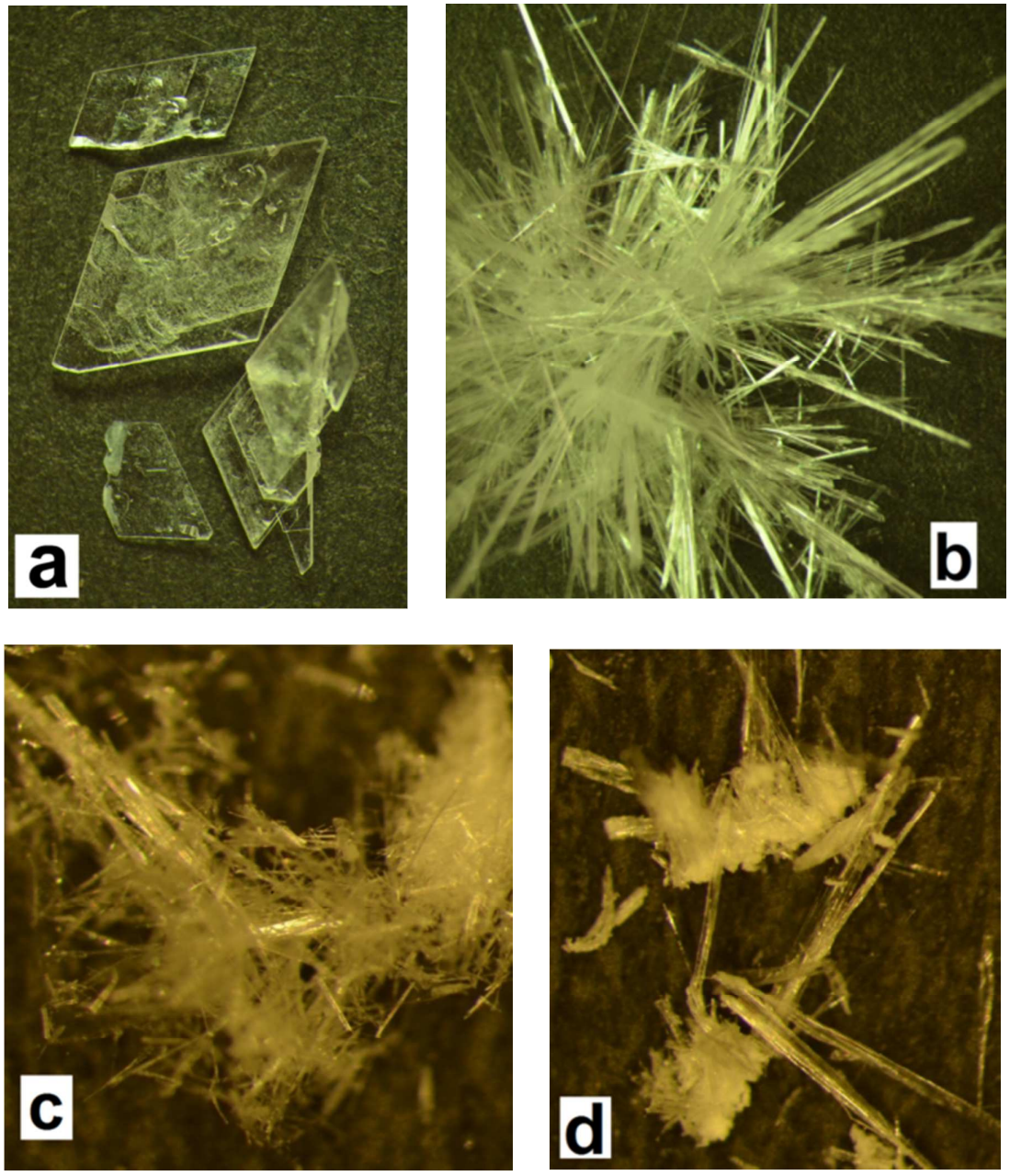

Figure 1. Microscopic pictures of scalemic and racemic crystalline samples of diol **1**: (**a**) prisms *rac*-**1**.**1** and (**b**) needles *rac*-**1**.**2** after room temperature slow crystallization of *rac*-**1** from cyclohexane/ EtOAc; (**c**) *rac*-**1**.**3** crystals after rapid *rac*-**1** crystallization from hot solution in light petroleum/EtOAc; (**d**) *scal*-**1** crystals from light petroleum/EtOAc.

The *rac*-**1**.**1** crystals clearly differ from other diol **1** crystalline modifications in their appearance. In order to clarify the relationships between all these modifications, we compared their infrared spectra recorded in the KBr matrix in pairs. The comparison itself is illustrated in Figure 2.

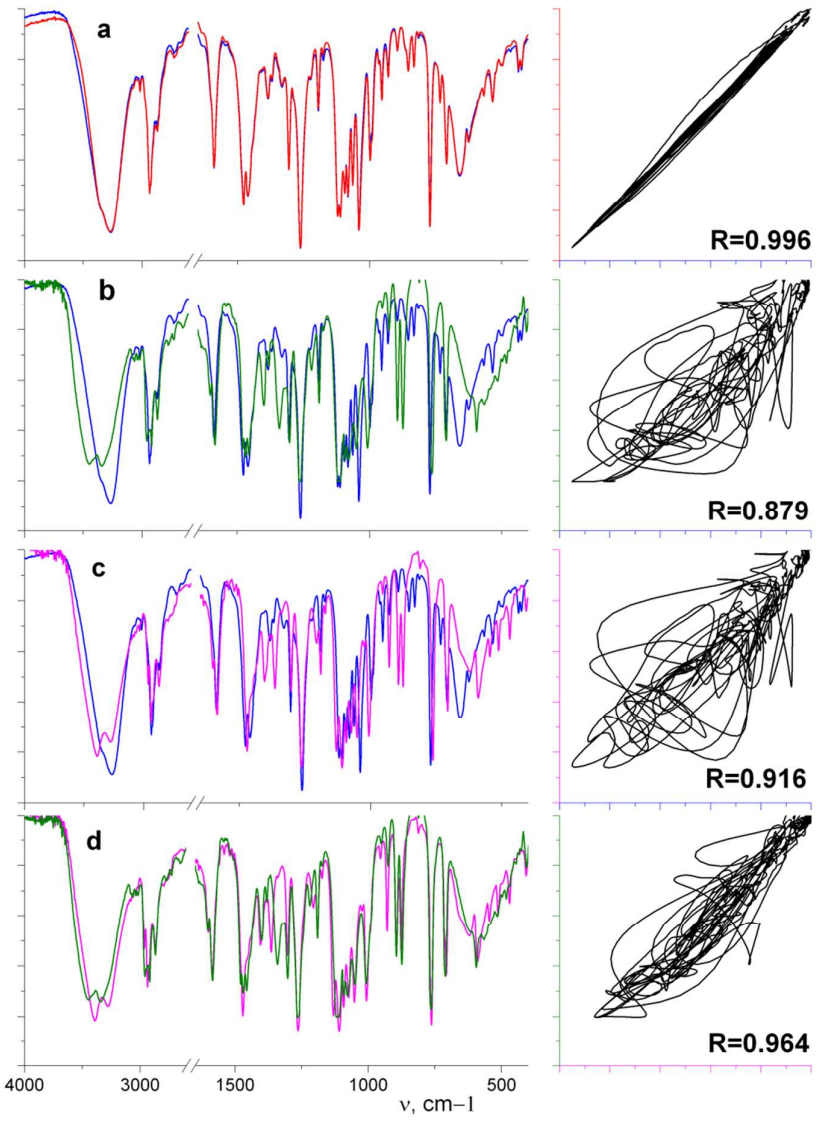

Figure 2. IR spectra in KBr pellets (on left) and their correlation trajectories (on right): (**a**) *rac*-**1.3** (red curve) against *scal*-**1**, in this case (*R*)-**1**, (blue curve); (**b**) (*rac*-**1.1** (olive) against (*R*)-**1** (blue); (**c**) *rac*-**1.2** (magenta) against (*R*)-**1** (blue); (**d**) *rac*-**1.1** (olive) against *rac*-**1.2** (magenta).

The left graph of each pair of drawings corresponds to the two compared IR spectra $A_1 = f(\nu)$ and $A_2 = f(\nu)$ (A_1, A_2 are the relative absorption of the samples for the same frequency ν), represented in the standard form. To quantify the degree of similarity, the standard statistical parameter, Pearson correlation coefficient $R = \frac{cov(A_1,A_2)}{\sigma_{A_1}\sigma_{A_2}}$, was used. The right graph in the drawings ("correlation trajectory") displays the parametric dependence A_1 vs A_2, which is a graphical representation of the correlation between the spectra and reflects the presence or absence of mutual agreement in the variation of the absorption of different samples when moving along the *v* scale. Obviously, if the two spectra are equally normalized and completely

similar, the correlation trajectory should degenerate into a straight line with the angle tangent equal to 1. If there are differences in the characteristic wavelengths and the extinctions of the absorption bands of the spectra being compared, then characteristic loops appear on the graph. Unlike the correlation coefficient *R*, which is an integral parameter, the graphical representation of the correlation between the spectra demonstrates the nature of the differences between them in compact and evident form, especially effective when it is necessary to quickly extract similar (or, alternatively, different) fragments in a large data set. Details of such an analysis have been described in our previous publications.[28,16]

As can be seen from the figure, the spectra of polycrystalline samples of *rac*-**1**.**3** and *scal*-**1** practically coincide, which indicates a significant sameness of their crystalline organization. For chiral compounds in which functional groups (in this case, primary and secondary hydroxyl groups of the glycerol fragment) capable of forming strong intermolecular hydrogen bonds are present, the coincidence of the spectra of enantiopure and racemic samples is most likely indicative that *rac*-**1**.**3** represents a racemic conglomerate, that is, a mechanical mixture of crystals, the organization of which coincides (or represents a mirror copy) with the (*R*)-**1** crystal packing. The coincidence of the spectra of *scal*-**1** and *rac*-**1**.**3** allows us to use only the scalemic sample for comparison purposes. As Figure 2 shows, all other pairs of spectra differ significantly. Consequently, *rac*-**1**.**1**, *rac*-**1**.**2** and *rac*-**1**.**3** samples have different crystal packings. X-ray analysis confirms this conclusion.

Single-crystal X-ray investigations. The unit cell of *rac*-**1**.**1** crystals contains a single symmetry independent molecule. This molecule and the numbering scheme adopted in the article are shown in Figure 3a. The unit cell belongs to the monoclinic centrosymmetric space group *C*2/c (Table 1). Already on this basis it is clear that *rac*-**1**.**1** crystals represent a normal racemic compound. The primary crystal-formative motif for this crystal packing is a 2D bilayer parallel to the *0bc* plane (Figure 3b). As it can be seen from the figure, the bilayer consists of infinite 1D ribbons formed by enantiomers with the same configuration. Its 2D structure is consolidated by infinite chains of intermolecular hydrogen bonds O1–H1···O'2 [*d* (O1···O'2) = 2.835(2) Å, ∠(O1H1O'2) = 172(2)°], O'2–H'2···O"1 [*d* (O'2···O"1) = 2.854(2) Å, ∠(O'2H'2O"1) = 160(2)°], O"1–H"1···O'"2, etc.

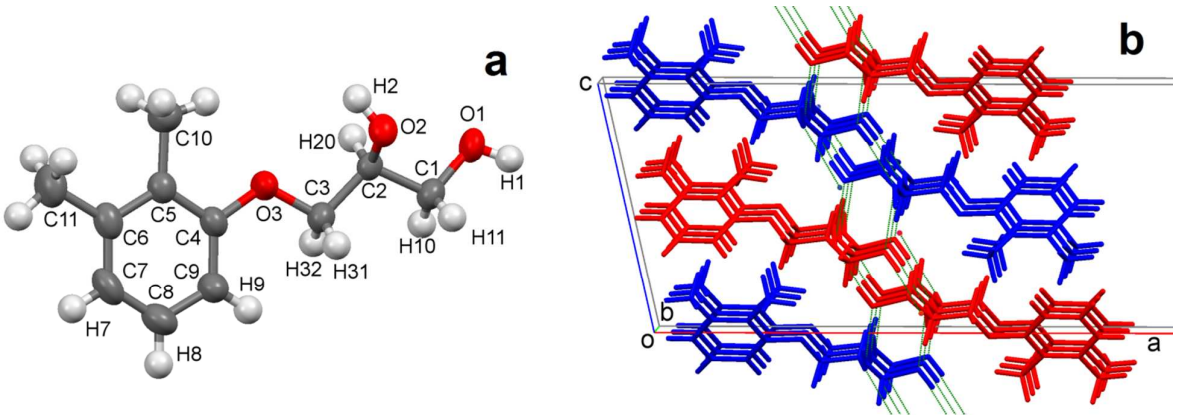

Figure 3. (**a**) Geometry of the symmetry independent *S*-molecule in the crystal of *rac*-**1.1** sample and numbering scheme adopted in the text. Non-hydrogen atoms are represented by probability ellipsoids of thermal vibrations (p = 50%), hydrogen atoms – by spheres of arbitrary radii. (**b**) Detail of the crystal packing for *rac*-**1.1**: 2D bilayer parallel to *0bc* plane; *R*-enantiomers are colored in red, *S*-enantiomers are colored in blue.

The *rac*-**1.2** crystals also belong to the centrosymmetric space group (Table 1, *P*-1, Z' = 1). That is, despite the fact that *rac*-**1.2** crystals with their needle shape are to some extent similar to the *rac*-**1.3** crystals (Figures 1b and 1c), the *rac*-**1.2** crystals represent the normal racemic compound, and hence this form is a polymorphic version of *rac*-**1.1**. The primary motif in *rac*-**1.2** crystals is a 1D column oriented along the *0a* axis (Figure 4). Two zigzag sequences of intermolecular H-bonds, O1–H1···O'2 [d (O1···O'2) = 2.782(3)Å, ∠(O1H1O'2) = 161(3)°] and O'2–H'2···O"1 [d (O'2···O"1) = 2.775(3)Å, ∠(O'2H'2O"1) = 173(2)°], link the alternating molecules of the opposite enantiomers to a single extended 1D system.

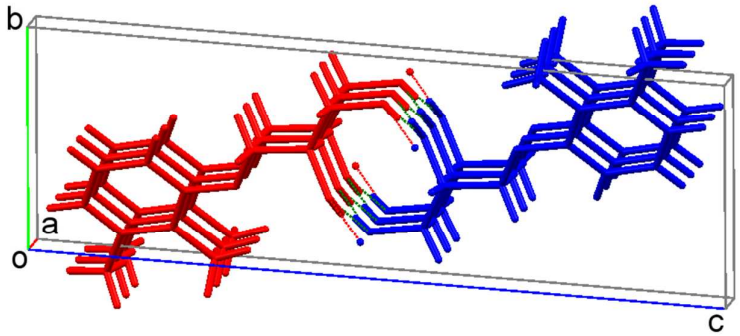

Figure 4. Detail of the crystal packing for *rac*-**1.2**: 1D column parallel *0a* direction.

X-ray diffraction analysis results for a single crystal picked at random from the polycrystalline *rac*-**1.3** sample are shown in Table 1 (where this crystal is designated as *S*-**1**). There are two independent molecules A and B in the asymmetric unit of the monoclinic $P2_1$ unit

cell of this crystal. Both molecules have common *S*-configuration, practically coinciding lengths of bonds and valence angles and differ only in the conformation of the glycerol fragment (see below). These molecules are shown in Figure 5.

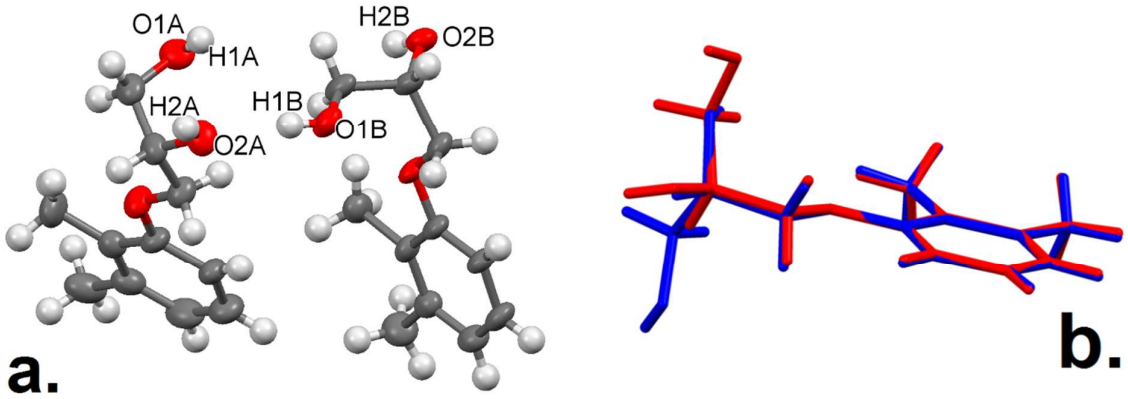

Figure 5. (**a**) Geometry of symmetry independent molecules in the crystal picked from *rac*-**1.3** polycrystalline sample. Non-hydrogen atoms are represented by probability ellipsoids of thermal vibrations (p = 30%), hydrogen atoms – by spheres of arbitrary radii. (**b**) Conditional superposition of the independent molecules; A molecule - red, B molecule - blue.

Crystallization of a racemate in the Sohncke group with any number of independent molecules with equal configuration guarantees the enantiomeric purity of an ideal single crystal and in this sense, is the proof of spontaneous resolution of a substance. X-ray diffraction analysis of a single crystal selected from the enantiopure *R*-**1** sample was brought to the establishment of unit cell parameters, which, to within an experimental error, coincided with those listed in Table 1 for *rac*-**1.3**, which confirms their general nature.

The primary supramolecular crystal-formative motif in *S*-**1** crystals is a 1D column formed around the 2_1 axis in the *0b* direction and consisting of alternating independent molecules A and B. We draw the readers' attention to the fact that one-dimensional supramolecular motifs are realized in the crystals *rac*-**1.2** and *rac*-**1.3** having an acicular habitus. The presence of a two-dimensional motif in the case of *rac*-**1.1** leads to a striking change in the habitus and the formation of plate-like crystals.

Let us return to the supramolecular motif in *scal*-**1** crystals. The molecules forming the column are interconnected by a system of intermolecular hydrogen bonds (IMHB) O–H···O'. The sequence of such IMHBs forms a left-handed *M*-helix in the case of a crystal formed by *S*-molecules. Eight molecules (four A and four B) fall inside one helix pitch. By all these indications, it coincides with the well-known for the TAGE family *mephenesin-like motif*.[15] In particular, it is present in the scalemic crystals of monomethylated analogs of diol **1**, *ortho*- and

meta-tolyl glycerol ethers **2** and **3** (Chart 1).[17] Details of the 1D supramolecular crystal-formative motif in *S*-**1** crystals are illustrated in Figures S1 and S2, ESI.

Spatial organization of the glycerol fragment in TAGE molecules is completely described by enumerating the conformations of the H1O1C1C2, O1C1C2C3, C1C2C3O3, C2C3O3C4, H2O2C2C3 и O2C2C3O3 fragments. In the non-racemic crystals of all the just mentioned diols **1**-**3**, conformational formulas for symmetry independent molecules A (*ap,-sc,-sc,ap,-sc,sc*) and B (*sc,sc,sc,ap,ac,ap*) turn out to be constant (angle signs are given for *R*-enantiomers). The numerical values of the corresponding torsion angles are also quite close, which indicates the similarity of the spiral structures of the primary supramolecular motifs for the molecules being compared. The main factor that destabilizes the mephenesin-like motif in the case of a meta-substituted derivative **3** is the close contact between the methyl groups in the spiral stacks.[17] This factor leads to an increase in the spiral pitch and, as a consequence, to a decrease in the packing density. It is easy to verify that in the case of 2,3-dimethyl derivative **1** this tendency is aggravated. The dimension of the full helix pitch of the supramolecular motif coincides with the *b* parameter of the $P2_1$ unit cell, common for all diols **1**-**3**. In the discussed series, this parameter is 4.8558(3) Å for mephenesin **2**, 4.9317(5) Å for *meta*-tolyl ether **3** and 5.037(6) Å for disubstituted diol **1**. The packing density of the crystals also decreases in the same sequence: the value of PI is 67.5% for *scal*-**2**, 65.5% for scal-**3** (68.6%) and 65.1% for *S*-**1**. (*rac*-**1**.**1** 69.9 %; *rac*-**1**.**2** 70.0 %)

With this information alone, one would expect that the homochiral packing, which is the only stable crystalline form in the case of mephenesin **2**, loses its advantages in the case of *meta*-tolyl glycerol ether **3** and, especially, in the case of 2,3-dimethylphenyl ether of glycerol **1**. This assumption is confirmed indeed in the case of compound **3**, which crystallizes from the racemic feed material in the heterochiral form of normal racemic compound. For *rac*-**3** sample PI is equal to 68.6% and the Gibbs energy of the racemic compound formation was found to be -2.70 kJ mol^{-1}.[17] This means that for *meta*-methyl derivative **3** an empirical regularity is valid, according to which racemates are denser than the corresponding enantiopure samples, so called *Wallach's rule*. (Or, if we comply with the historical justice, *Liebisch's rule*, as it is suggested in the informative article of Ernst.[29]) However, in the same work in which the term "*Wallach rule*" first appeared, it was shown that the rule is not absolute and contains numerous exceptions.[30] Subsequently, this conclusion was repeatedly confirmed in the study of crystals of homogeneous[31,32] and dissimilar[33] arrays of chiral organic compounds.

The crystallization of diol **1** discussed herein has much in common with the crystallization of 3-phenyllactic acid, studied in the Navare and MacDonald paper.[13] In both cases, racemic conglomerate and several polymorphs of racemic compound can crystallize from the racemic

feed material depending on the conditions. In both cases, Wallach's rule is formally observed, and homochiral crystals are less dense than racemic crystals. But the firsts melt at higher temperatures.

In order to analyze the reasons for preferences in the process of *rac* vs *scal* crystallization, the series of compounds **2** – **3** - **1** is of particular interest since, with the general supramolecular motif retaining for homochiral crystals throughout the entire series and the monotonic decrease in density noted for them, the nature of the stable form of the crystals, *scal* - *rac* – *scal*, changes during the cross-over from compound to compound. Such an analysis involves the use of high-level calculations and goes beyond the scope of this paper. But in any case, for its verification, such analysis requires some reference points related to the energy of the crystals.

Generally speaking, taken by themselves, the data of the X-ray experiments do not provide a basis for establishing energy preferences for one or another compound. We tried to do this in other ways.

Thermal investigations of the stable and metastable crystalline diol 1 forms. Figure 6 shows the DSC thermograms of diol **1** samples obtained by crystallization from solutions. As it can be seen from the figure, the melting of the scalemic sample (blue curve, T_{f_R}=102.8 ^{o}C) is characterized by a single peak of regular shape. Further experience has shown that the crystalline enantiopure samples obtained under different conditions from the solution, as well as the crystallization products of enantiopure melts, exhibit the same monomodal melting peak when heated. Most likely, the scalemic diols **1** in the system under investigation are characterized by the only described above type of crystal packing. Consequently, on the racemic samples thermograms, the one and only one endothermic process, namely the peak $T_{f_{R+S}}$= 81.1 ^{o}C for *rac*-**1**.**3** sample (Figure 6, red curve), can be attributed to the eutectic (racemic conglomerate) melting. All other observed endothermic peaks cannot belong to eutectics of enantiopure phases with a different crystal structure. This means that the bimodal character of the melting curves of *rac*-**1**.**1** (olive) and *rac*-**1**.**2** (magenta) samples indicates the presence of two racemic phases in each sample. A phase with a lower melting point (T_{f_α}=76.5 ^{o}C; henceforth referred to as *α-rac*) dominates in the *rac*-**1**.**2** sample. Accordingly, the phase of the racemic polymorph with the higher melting point (T_{f_β}=79.8 ^{o}C), prevailing in the *rac*-**1**.**1** sample, will be denoted as *β-rac*.

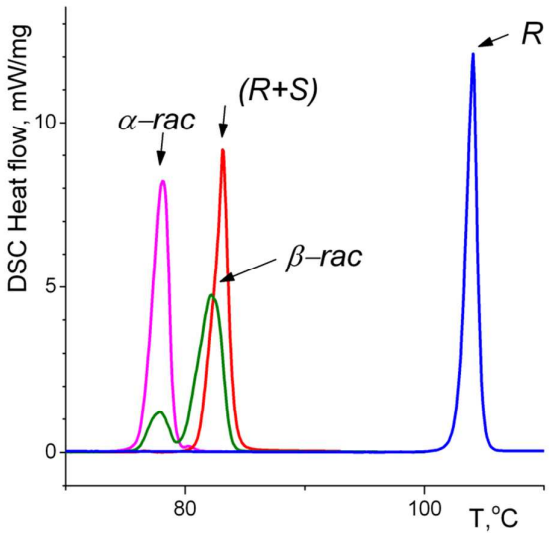

Figure 6. Experimental DSC traces of the polycrystalline diol **1** samples, obtained by solution crystallization. The blue curve characterizes the melting of enantiopure *R*-**1** sample, red curve - racemic conglomerate, olive - *rac*-**1**.**1**, magenta - *rac*-**1**.**2**. Explanations in the text.

When the dry *rac*-**1**.**1** crystals are stored at room temperature, the *β-rac* phase is stable for a long time, but in the solvent (MTBE) medium at 20 °C, the plate-like crystals break down fairly quickly, and phase *β-rac* transforms to *α-rac*.

The melting thermograms are significantly more complicated for the racemic samples obtained by melt crystallization. A full shape of the thermograms and a detailed description of the experiments are given in ESI, Figures S3 and S4. Here we will outline the main results. Thus, on the thermogram of *rac*-**1** sample, which was previously melted and then cooled to 20 °C (Fig. 7, orange curve), a melting peak was observed at 79.8 °C, identical in its thermochemical parameters to the melting peak of *β-rac* phase. It is preceded by fluctuations in the baseline, indicating that this phase is formed during the recrystallization of some independent intermediate phase (denoted as *γ-rac*). If the melt, after cooling to 20 °C, was subjected to an additional heating cycle of up to 62 °C to complete the recrystallization process, followed by cooling, then on the thermogram of the sample with such history the only melting peak for *β-rac* phase was observed (Fig. 7, olive curve).

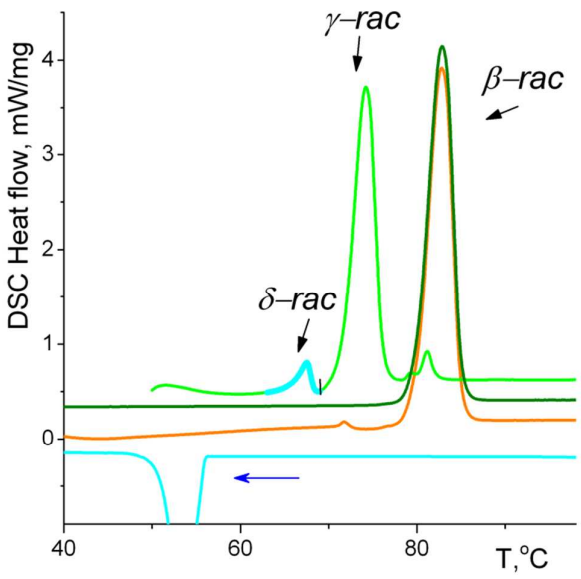

Figure 7. Experimental DSC traces of the crystalline forms of diol 1 obtained by crystallization from a melt. Green curve - a sample for which the melting cycle is commenced immediately upon completion of crystallization at 50 °C; orange curve - a sample cooled after crystallization to 20 °C; olive - a similar sample, additionally held at 60 °C to complete the recrystallization before the melting cycle. Cyan curve - crystallization of the sample upon cooling, as well as a fragment of the heating cycle corresponding to melting

The *γ-rac* phase can be observed experimentally if the heating cycle begins immediately after the crystallization of the racemic melt (Fig. 7, green curve). Under these conditions, its melting peak at 71.5 °C becomes the main element of the thermogram, which makes it possible to evaluate the thermochemical characteristics of this phase. The minor bimodal signal at higher temperatures can be described by a combination of the *β-rac* and the conglomerate melting.

On the same thermogram, an additional minor endothermic peak (marked by cyan color) is observed at 65.6 °C. It suggests that another relatively stable phase of the racemic composition, *δ-rac*, is present in the melting sample. Comparison of the crystallization enthalpy of the racemic sample (the lowest cyan curve, ΔH_f = 17.0 kJ mol^{-1}) and the melting enthalpy of *γ-rac* (ΔH_{f_γ} = 23.6 kJ mol^{-1}) demonstrates a significant deficit in the enthalpy within crystallization/melting cycle. This suggests that the *δ-rac* phase is the first to form during the crystallization of the melt, and then rapidly recrystallizes to the *γ-rac* phase, which is accompanied by an exothermic effect. The base-line shift observed on the thermogram in the temperature range 55-65 °C confirms this hypothesis. Then the observed minor endothermic peak can be attributed to the melting of the

residual amounts of the *δ-rac* phase, which did not have time to recrystallize into *γ-rac*. Indirect information obtained in additional DSC experiments (ESI, Figure S4) suggests that the *δ-rac* phase is a metastable ideal solid solution. Unfortunately, the short time of transformation of the *γ-rac* and *δ-rac* phases makes it difficult to observe them under other conditions, except directly in the DSC experiment, and accordingly the identification of their nature by independent methods.

The final experimental thermochemical characteristics of all the identified crystalline forms of compound **1** are shown in Table 2.

Table 2. DSC measured temperatures (T), enthalpies (ΔH), and entropies ΔS of fusion for distinct crystalline diol **1** forms

	T_f (°C)	ΔH_f (kJ mol^{-1})	ΔS_f (J mol^{-1} K^{-1})
R-**1**	102.8	35.1	93.2
(*R*+*S*)-**1**	81.1	32.1	90.5
α-rac-**1**	76.5	32.9	94.1
β-rac-**1**	79.8	29.1	82.3
γ-rac-**1**	71.5	23.6	68.3
δ-rac-**1**	65.6	17.0	50.2

Energetic preferences of the crystalline diol 1 forms. As noted above, the *δ-rac* phase is unstable and rapidly turns into the *γ-rac* phase during the heating of *rac*-**1** samples crystallized from the melt. The *γ-rac* phase also spontaneously recrystallizes into *β-rac*. The *β-rac* phase can exist for a sufficiently long time in a dry state, but in a solvent medium at room temperature it recrystallizes into *α-rac*. The relative thermodynamic stability of the *α-rac* phase and the racemic conglomerate is not so obvious. In spite of the fact that the conglomerate has a higher melting point, pure dry samples of the both phases at room temperature can exist for a long time (at least a week) in an unchanged form. Even with active slurrying of the corresponding individual samples in hexane medium during 24 hours at 20 °C they do not exhibit any appreciable transformations. For example, the thermograms and IR spectra of the samples before and after slurrying remain unchanged.

A quantitative representation about the relative thermodynamic stability of all the phases of racemic composition revealed can be obtained by constructing the energy diagram of the system under study, which reflects variations of the enthalpies, entropies, and Gibbs energies of these phases as a function of temperature. For each phase the difference of the thermodynamic

functions by heating a crystalline sample from the initial temperature $\boldsymbol{T0}$ to the fusion temperature $\boldsymbol{T^f}$ and further to the final temperature of a melt $\boldsymbol{T1}$ can be represented as

$$\Delta \boldsymbol{H^{T0/T1}} = \begin{cases} \int_{\boldsymbol{T0}}^{\boldsymbol{T1}} \boldsymbol{C_p^{solid}}(\boldsymbol{T})\boldsymbol{dT}\ , \boldsymbol{T1} < \boldsymbol{T^f} \\ \int_{\boldsymbol{T0}}^{\boldsymbol{T^f}} \boldsymbol{C_p^{solid}}(\boldsymbol{T})\boldsymbol{dT} + \Delta \boldsymbol{H_f} + \int_{\boldsymbol{Tf}}^{\boldsymbol{T1}} \boldsymbol{C_p^{lq}}(\boldsymbol{T})\boldsymbol{dT}\ , \boldsymbol{T1} \geq \boldsymbol{T^f} \end{cases}$$

$$\Delta \boldsymbol{S^{T0/T1}} = \begin{cases} \int_{\boldsymbol{T0}}^{\boldsymbol{T1}} \frac{\boldsymbol{C_p^{solid}}}{\boldsymbol{T}}(\boldsymbol{T})\boldsymbol{dT}\ , \boldsymbol{T1} < \boldsymbol{T^f} \\ \int_{\boldsymbol{T0}}^{\boldsymbol{T^f}} \frac{\boldsymbol{C_p^{solid}}}{\boldsymbol{T}}(\boldsymbol{T})\boldsymbol{dT} + \frac{\Delta \boldsymbol{H_f}}{\boldsymbol{T^f}} + \int_{\boldsymbol{Tf}}^{\boldsymbol{T1}} \frac{\boldsymbol{C_p^{lq}}}{\boldsymbol{T}}(\boldsymbol{T})\boldsymbol{dT}\ , \boldsymbol{T1} \geq \boldsymbol{T^f} \end{cases}$$

$$\Delta \boldsymbol{G^{T0/T1}} = \Delta \boldsymbol{H^{T0/T1}} - \boldsymbol{T1} \cdot \Delta \boldsymbol{S^{T0/T1}}.$$

Measurements of the effective heat capacities of the experimentally accessible samples by DSC method were carried out with the use of samples of increased mass (~ 10 mg). The corresponding thermograms are shown in Figure 8.

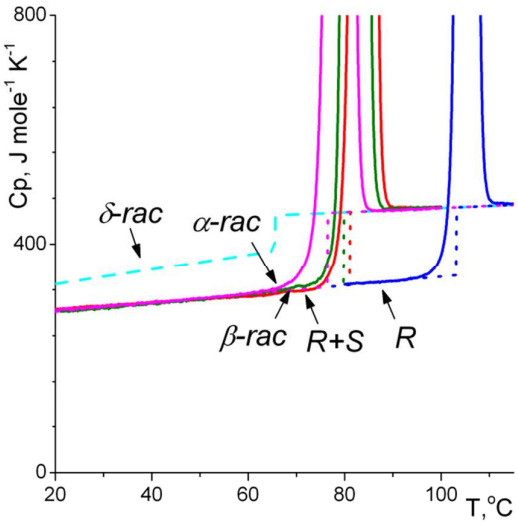

Figure 8. DSC curves presenting the effective heat capacity of racemic samples of different phase compositions. Blue, red, olive, magenta and cyan lines correspond to *R*-**1**, racemic conglomerate, *β-rac*, *α-rac* and *δ-rac* phases. The dotted lines show the extrapolated values of the heat capacity of individual phases in the region of solid/melt phase transitions. For δ-*rac* phase, the dashed line corresponds to the extrapolated values obtained from the crystallization thermogram (see text).

Note that the heat capacities of the *α-rac*, *β-rac*, enantiopure phases and racemic conglomerate in the temperature range from 20 °C to the melting temperatures turned out to be close to each other within the experimental accuracy. For the *δ-rac* phase, the heat capacity and melting enthalpy were determined from the thermogram of crystallization of a preliminarily

melted racemic sample. As noted above, *γ-rac* phase was intermediate between *δ-rac* and *β-rac* and quickly turned into the latter. Therefore, it was not possible to measure experimentally its heat capacity. To calculate the thermodynamic potentials of this phase and schematically display them on the general energy diagram, the *Cp* value was used which was the mean between those for *δ-rac* and *β-rac*. We note that the variation of this parameter in the entire range between the heat capacities of *δ-rac* and *β-rac* does not introduce qualitative changes into the observed picture.

In the absence of absolute values for standard thermodynamic potentials, the enthalpy and the entropy of *α-rac* phase at 20 °C were taken as conventional zero. Obtained relationships are graphically illustrated in Figure 9.

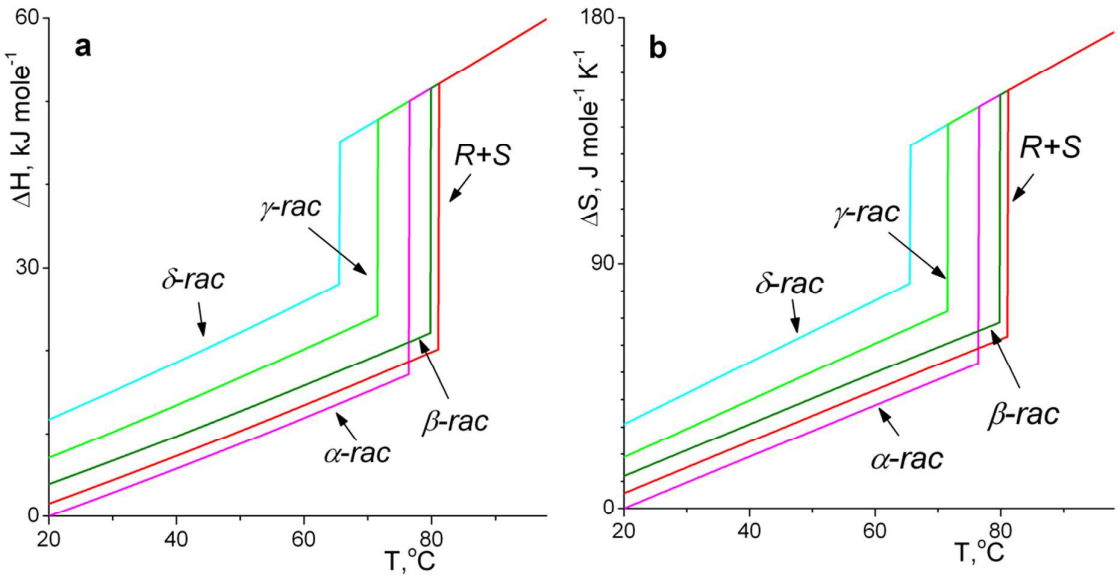

Figure 9. Dependences of the relative enthalpies (*a*) or entropies (*b*) of conglomerate (red), *α-rac*-**1** (magenta), β-*rac*-**1** (olive), *γ-rac*-**1** (green) and *δ-rac*-**1** (cyan) on temperature.

On the basis of these graphs, the dependences of the changes in the free Gibbs energies of these phases on temperature have been plotted (Figure 10). It should be remembered that we know only the relative changes in enthalpy and entropy. For this reason, the changes in Gibbs energy were calculated as follows:

$$\boldsymbol{\Delta G_x^T = \left(H_x^T - H_{\alpha-\mathrm{rac}}^{20^oC}\right) - T\left(S_x^T - S_{\alpha-\mathrm{rac}}^{20^oC}\right) = \left(H_x^T - T \cdot S_x^T\right) - \left(H_{\alpha-\mathrm{rac}}^{20^oC} - T \cdot S_{\alpha-\mathrm{rac}}^{20^oC}\right),}$$

which is equivalent to calculating the Gibbs energy of each phase relative to the hypothetical system, the enthalpy and entropy of which coincides with the values of these parameters for the

α-rac phase at 20 °C. This does not affect the relative position of the curves and the characteristic points on the graph, but, to avoid misinterpretation, it should be taken into account that with such a transformation, the tangent of the tangent line for the $\boldsymbol{\Delta G_x^T}$ plot is not reflecting the proper entropy of this phase, but is equal to value $\boldsymbol{S_x^T - S_{\alpha-rac}^{20^oC}}$. In particular, for $\boldsymbol{\Delta G_{\alpha-rac}^T}$ the tangent line at 20 °C is horizontal.

It is seen from Fig. 10 that in the entire accessible temperature range the *γ-rac* and *δ-rac* phases are metastable and substantially inferior in energy to all other crystal modifications of compound **1** known to us. Obviously, their formation during the crystallization process is due to kinetic reasons, such as the ease and efficiency of the nucleation stage in the formation of *δ-rac* and the relatively low potential barrier of solid-phase recrystallization of *δ-rac* into *γ-rac*. Further, *γ-rac* in the solid phase is almost as easily transformed into *β-rac*. The ease of implementation of such a cascade of solid-phase transformations at near to room temperatures suggests that these three phases are characterized by a similar crystal structure. Under this condition, the transformations do not need a significant rearrangement of the crystal packing, but at each stage it is possible to obtain a noticeable gain in energy.

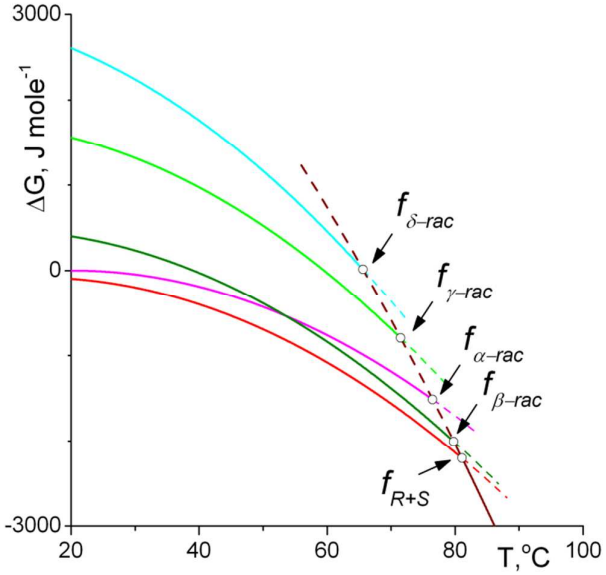

Figure 10. Dependences of the relative Gibbs free energies on temperature for different phases of racemic composition. Red line – conglomerate, magenta - *α-rac*-**1,** olive - *β-rac*-**1**, green - *γ-rac*-**1**, cyan- *δ-rac*-**1**, brown – stable (solid line) and metastable supercooled (dashed) racemic liquid.

The *α-rac* and *β-rac* phases are energetically very close to each other and to racemic conglomerate, so the energy relations of these three crystalline modifications are more complex. Table 3 shows the calculated values of the free energies of the phase transitions $\Delta G_{ss(RS)}$ between the racemic conglomerate and other racemic phases at a temperature of 20 °C and at the melting point of the corresponding phase. From these data and from Figure 10 it follows that the thermodynamically preferred way of crystallization of *rac*-**1** in the investigated temperature range (from 20 °C to the melting temperature) is a conglomerate. At the melting temperature, the *α-rac* phase is thermodynamically the least preferred among the three discussed ways of the racemate crystallization. At the same time, this phase has the greatest value of the melting enthalpy, and, accordingly, the lowest entropy in the crystalline state. An important consequence of this fact is that as the temperature is lowered, the Gibbs potential of *α-rac* grows more slowly than that of *β-rac* and also that of the conglomerate. At circa 53.5 °C this phase becomes more stable than *β-rac*. Unfortunately, we failed to detect this formally enantiotropic transition experimentally. We believe that the reason is the high potential barrier of the corresponding solid-phase rearrangement of essentially different (Figures 3 and 4) crystal packings.

It also follows from Figure 10 that below the room temperature the *α-rac* phase should become more stable than racemic conglomerate. It should be noted here that the very difference in the calculated values of the free energy of *α-rac* and the conglomerate at the near room temperatures (Table 3) is very small, $\Delta G^{20°C}_{(R+S)/\alpha} < 100$ J mol^{-1}. This value is quite comparable with the experimental error of DSC measurements, and therefore the question of the thermodynamically stable state of the system at room temperature cannot be uniquely resolved only on the basis of the data under consideration.

Table 3. Calculated values of the free energy of the phase transition $\Delta G_{ss(RS)}$ between the racemic conglomerate and other racemic modifications of compound **1**

Phase	$\Delta G^{20°C}_{ss(RS)}$, kJ mol^{-1}	$\Delta G^{Tf}_{ss(RS)}$, kJ mol^{-1}
α-rac	0.097	0.41
β-rac	0.497	0.12
γ-rac	1.66	0.85
δ-rac	2.70	1.35

To clarify the thermodynamically advantageous way of crystallization of *rac*-**1** under these conditions, we realized a direct experiment: equal amounts (~ 10 mg) of the racemic conglomerate and the *α-rac* phase were mixed, suspended in hexane and subjected to vigorous

stirring for 4 hours. The initial state of each of the components and the final composition of the system were controlled by DSC and IRS methods. It was found that, at the end of the mixing, the precipitate consisted of a pure racemic conglomerate, there was no evidence of the presence of the *α-rac* phase in it. This indicates that spontaneous recrystallization of the racemic *α-rac* compound into a racemic conglomerate takes place under these conditions, and therefore it is the conglomerate that remains the thermodynamically most advantageous state of the system at 20 °C and above.

In a sense, the result of the slurrying experiment comes into conflict with the experimentally established long-term stability of dry *α-rac* samples. To clarify the situation, we undertook a series of experiments on the crystallization of diol **1** samples of various enantiomeric compositions. Figure 11 shows the results of these tests.

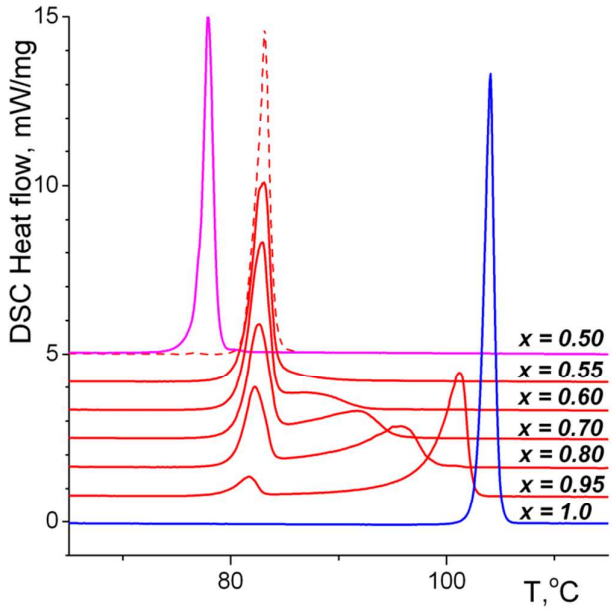

Figure 11. Thermograms of dry crystalline precipitates obtained by evaporating solutions of compound **1** samples of different enantiomeric composition in MTBE. Blue color denotes an enantiopure sample, x = 1.0; magenta stands for racemic sample, x = 0.50. Red dashed curve is the thermogram of the sample of indubitable racemic conglomerate; solid red curves from top to bottom correspond to the original compositions x = 0.55, 0.60, 0.70, 0.80, 0.95 (x are the mole fractions of the predominant enantiomer).

Judging by the thermochemical parameters of the corresponding peak, the crystallization of **1** from a solution of a strictly racemic composition leads to the precipitation of a practically pure *α-rac* phase. Obviously, such a result is determined by kinetic factors. But the presence of even a small excess of one of the enantiomers in the system leads to the crystallization of the racemic part of the precipitate exclusively in the form of a conglomerate. This is indicated by the

presence on the thermograms for x = 0.55÷095 of a characteristic peak of the corresponding eutectic.

Racemic 3-(2,3-dimethylphenoxy)propane-1,2-diol, compound 1 could be resolved by direct entrainment procedure. To a certain extent, our study of the phase behavior of compound **1** was inspired by the propinquity of its chemical structure to the structure of the known API *xibenolol* (Chart 1, structure **5**). On the one hand, the ability of *rac*-**1** to spontaneous resolution during crystallization, discovered by us, opens the principle possibility of using direct methods to obtain its individual enantiomers.[34] In case of success, nonracemic **1** can serve as a useful precursor in the synthesis of nonracemic **5**. On the other hand, the complex phase behavior of **1** and, in particular, the presence of several energy-close (meta)stable crystalline racemic compounds generally negatively affects the results of direct resolution.[35,7] Nevertheless, two facts, revealed as a result of our research, allowed us to hope for success. First, the racemic conglomerate, at least above room temperature, proved to be thermodynamically more advantageous than all polymorphic racemic compounds. Secondly, it is this form that crystallizes primarily under the condition of initial enantiomeric enrichment of the sample.

With this in mind, we realized a successful demonstration experiment of *rac*-**1** resolution by entrainment. We used water as a solvent. The concentration of saturated *rac*-**1** solution at 52 °C determined by the polythermal method was C_{sat} = 10.7 mg/ml, and for (*R*)-**1** C_{sat} = 5.3 mg/ml. This means that under these conditions the Meyerhoffer rule is well observed. For these samples, the inverse to dissolution spontaneous crystallization becomes noticeable at 39 °C in the first case, and at 30 °C in the second.

For the demonstration experiment, we used slightly enriched (~ 10% *ee*) near racemic diol **1**. For such a sample, the concentration of the saturated solution was 8.5 mg/ml at 50 °C, and spontaneous crystallization began at 29.5 °C. Crystallization, stimulated with enantiopure seed crystals, was carried out at 37.5 °C. Other details of the process are given in the experimental part. For monitoring the entrainment abilities of diol **1** during seed induced crystallization we have used mother liquor enantiomeric composition measured by HPLC (Figure 12).

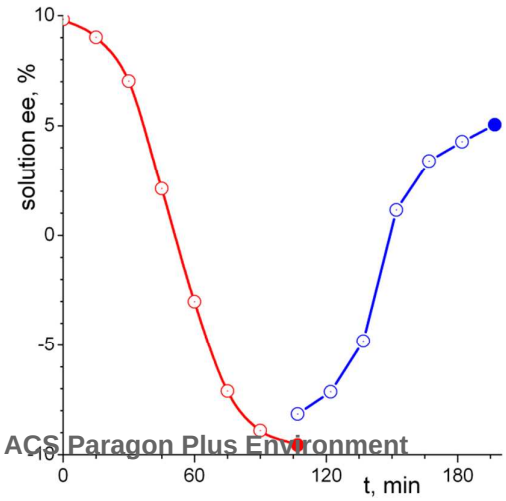

Figure 12. Mother liquor enantiomeric excess vs time in full cycle of preferential crystallization of diol **1** (red curve - 1-st run; blue - 2-nd run). Solid circles indicate the values of the enantiomeric excess at which the process was interrupted. Time for technical operations between runs is omitted.

As follows from the figure, during the crystallization process, the primary enantiomeric excess of solute (9.8%) decreased to zero, changed sign, and raised up to 9.5% in the opposite direction. At this point the process was interrupted. After separation of the precipitate, a missing amount of the racemate was added to the mother liquor. In the second run, the enantiomeric excess of the mother liquor crosses zero and reaches only 5.1% as maximum value. Therefore, for maintaining the entrainment procedure as a robust multi-cyclic process, to restore the starting enantiomeric enrichment of the near-racemic diol to about 10% after separation of the enantiomeric precipitate, a small amount of *scal*-**1** must be added to the mother liquor along with the racemate.

CONCLUSIONS

It has been established that the chiral phenyl glycerol ether bearing two methyl groups in the *ortho* and *meta* positions of the phenyl ring, 3-(2,3-dimethylphenoxy)propane-1,2-diol **1**, crystallizes from the racemic feed medium with the formation of at least five crystalline modifications: *α-rac*, *β-rac*, *γ-rac*, *δ-rac* racemic compounds and racemic conglomerate (R+S). The first two and the last modifications are formed during crystallization from solutions and form sufficiently stable in dry form monocrystals of satisfactory quality. The nature of these modifications has been revealed by X-ray diffraction analysis. Additional metastable phases *γ-rac* and *δ-rac* are formed during the crystallization of *rac*-**1** from melt. This fact has been detected by DSC method. The thermochemical characteristics (T_f, ΔH_f, ΔS_f and $C_p(T)$) have been measured for all the modifications found and for the racemic liquid phase, and graphs of the dependence of free Gibbs energy on temperature have been constructed on this basis.

It has been shown that the *δ-rac* phase is unstable and rapidly turns into *γ-rac* phase during heating of *rac*-**1** samples obtained from the melt. Further, *γ-rac* phase also spontaneously recrystallizes into *β-rac*. The *β-rac* phase can exist for a long time in a dry state, but in a solvent medium it is converted to *α-rac* already at room temperature. From the dependences $\Delta G.vs.T$ it follows that the *β-rac* and *α-rac* phases are capable of enantiotropic transition at a temperature of about 50 °C, however, we failed to detect that transition for dry samples.

At temperatures above 20 °C, the most thermodynamically stable crystal modification of *rac*-**1** is the racemic conglomerate (R+S). Nevertheless, in the case of the crystallization of *rac*-**1**

from solutions at room temperature, the racemic compound *α-rac* is formed, which is stable both in dry form and in solutions. But even a small excess of one of the enantiomers in the mother liquor leads to the fact that the entire racemic part of the crystallizing sample is precipitated in the form of a racemic conglomerate.

Taking into account that above room temperature the conglomerate is thermodynamically more favorable than all polymorphic racemic compounds, and that this particular form crystallizes from solutions under the condition of initial enantiomeric enrichment of the sample, we realized a successful demonstration experiment on the resolution of *rac*-**1** into individual enantiomers by the method of entrainment.

ASSOCIATED CONTENT

Supporting Information

The Supporting Information is available free of charge on the ACS Publications website at DOI:

Synthetic procedures, details of crystal packing in *S*-**1** crystals, and additional DSC experiments.

AUTHOR INFORMATION

Corresponding Author

* Tel.: +7 843 2727393; fax: +7 843 2731872.

E-mail address: baa@iopc.ru (A.A. Bredikhin)

Author Contributions

The manuscript was written through contributions of all authors. All authors have given approval to the final version of the manuscript.

Notes

The authors declare no competing financial interest.

ACKNOWLEDGMENTS

The authors thank the Russian Fund of Basic Research and the Government of the Republic of Tatarstan for partial financial support (Grant No. 15-43-02238).

REFERENCES

(1) Bernstein, J. *Polymorphism in molecular crystals*; Oxford University Press: New York, 2002, 410 pp.

(2) Bernstein, J. Polymorphism − a perspective. *Cryst. Growth Des.* **2011**, *11*, 632–650.

(3) *Polymorphism in pharmaceutical solids*; Brittain, H. G., Ed.; Informa Healthcare USA: New York, 2009, 480 pp.

(4) *Polymorphism: in the pharmaceutical industry*; Hilfiker, R., Ed.; Wiley-VCH: New York, 2006, 433 pp.

(5) Aitipamula, S.; Chow, P. S.; Tan, R. B. H. Conformational polymorphs of a muscle relaxant, metaxalone. *Cryst. Growth Des.* **2011**, *11*, 4101–4109.

(6) Stephenson, G. A.; Kendrick, J.; Wolfangel, C.; Leusen, F. J. J. Symmetry breaking: polymorphic form selection by enantiomers of the melatonin agonist and its missing polymorph. *Cryst. Growth Des*. **2012**, *12*, 3964-3976.

(7) Brandel, C.; Amharar, Y.; Rollinger, J. M.; Griesser, U. J.; Cartigny, Y.; Petit, S.; Coquerel, G. Impact of molecular flexibility on double polymorphism, solid solutions and chiral discrimination during crystallization of diprophylline enantiomers. *Mol. Pharm*. **2013**, *10*, 3850–3861.

(8) Braga, D.; Chelazzi, L.; Grepioni, F.; Nanna, S.; Rubini, K.; Curzi, M.; Giaffreda, S.; Saxell, H. E.; Bratz, M.; Chiodo, T. Imazamox: a quest for polymorphic modifications of a chiral and racemic herbicide. *Cryst. Growth Des.* **2014**, *14*, 1430–1437.

(9) Gubaidullin, A. T.; Samigullina, A. I.; Bredikhina, Z. A.; Bredikhin, A. A. Crystal structure of chiral *ortho*-alkyl phenyl ethers of glycerol: true racemic compound, normal, false and anomalous conglomerates within the single five-membered family. *CrystEngComm* **2014**, *16*, 6716–6729.

(10) Carvalho, P. S.; Ellena, J.; Yufit, D. S.; Howard, J. A. K. Rare case of polymorphism in a racemic fluoxetine nitrate salt: phase behavior and relative stability. *Cryst. Growth Des.* **2016**, *16*, 3875–3883.

(11) Fayzullin, R. R.; Zakharychev, D. V.; Gubaidullin, A. T.; Antonovich, O. A.; Krivolapov, D. B.; Bredikhina, Z. A.; Bredikhin, A. A. Intricate phase behavior and crystal structure features of chiral *para*-methoxyphenyl glycerol ether forming continuous and partial solid solutions. *Cryst. Growth Des.* **2017**, *17*, 271–283.

(12) Levkin, P. A.; Torbeev, V. Y.; Lenev, D. A.; Kostyanovskii, R. G. Homo- and heterochirality in crystals. *Top. Stereochem*. **2006**, *25*, 81–134.

(13) Navare, P. S.; MacDonald, J. C. Investigation of Stability and Structure in Three Homochiral and Heterochiral Crystalline Forms of 3-Phenyllactic Acid. *Cryst. Growth Des.* **2011**, *11*, 2422–2428.

(14) Zhang, C. C.; Matzger, A. J. A newly discovered racemic compound of pioglitazone hydrochloride is more stable than the commercial conglomerate. *Cryst. Growth Des.* **2017**, *17*, 414–417.

(15) Bredikhin, A. A.; Bredikhina, Z. A.; Zakharychev, D. V. Crystallization of chiral compounds: thermodynamical, structural and practical aspects. *Mendeleev Commun*. **2012**, *22*, 171–180.

(16) Bredikhin, A. A., Bredikhina, Z. A. Stereoselective crystallization as a basis for single-enantiomer drug production. *Chem. Eng. Technol*. **2017,** *39***,** DOI: 10.1002/ceat.201600649

(17) Bredikhin, A. A.; Zakharychev, D. V.; Bredikhina, Z. A.; Gubaidullin, A. T.; Fayzullin, R. R. Crystal structure and phase behavior of the tolyl glycerol ethers. From the conglomerate former to the chirality-driven nanogelator. *CrystEngComm* **2012**, *14*, 211–222.

(18) Bredikhina, Z. A.; Kurenkov, A. V.; Krivolapov, D. B.; Bredikhin, A. A. Stereoselective crystallization of 3-(2,6-dimethylphenoxy)propane-1,2-diol: preparation of the single-enantiomer drug mexiletine. *Tetrahedron: Asymmetry* **2015**, *26*, 577–583.

(19) Sayyed, I. A.; Thakur, V. V.; Nikalje, M. D.; Dewkar, G. K.; Kotkar, S. P.; Sudalai, A. Asymmetric synthesis of aryloxypropanolamines via OsO_4-catalyzed asymmetric dihydroxylation. *Tetrahedron* **2005**, *61*, 2831–2838.

(20) Ludwig, B. J.; West, W. A.; Currie, W. E. Muscle-paralyzing compounds related to mephenesin. *J. Am. Chem. Soc.* **1952**, *74*, 1935–1939.

(21) The Merck Index, 14th ed., Ed. M. J. O'Neil, Merck and Co., Inc., Whitehouse Station, NJ, USA, 2006, entry 10075.

(22) Kong, X.-D.; Ma, Q.; Zhou, J.; Zeng, B.-B.; Xu, J.-H. A smart library of epoxide hydrolase variants and the top hits for synthesis of (*S*)-β-blocker precursors. *Angew. Chem. Int. Ed.* **2014**, *53*, 6641–6644.

(23) Sheldrick, G. M. *SADABS, Program for Empirical X-ray Absorption Correction*; Bruker-Nonius: Delft, the Netherlands, 2004.

(24) Sheldrick, G. M. A short history of SHELX. *Acta Crystallogr. A* **2008**, *64*, 112–122.

(25) Farrugia, L. J. WinGX suite for small-molecule single-crystal crystallography. *J. Appl. Cryst.* **1999**, *32*, 837–838.

(26) Macrae, C. F.; Edgington, P.R.; McCabe, P.; Pidcock, E.; Shields, G.P.; Taylor, R.; Towler, M.; van de Streek, J. Mercury: visualization and analysis of crystal structures. *J. Appl. Crystallogr*. **2006**, *39*, 453–459.

(27) Spek, A. L. Single-crystal structure validation with the program PLATON. *J. Appl. Crystallogr*. **2003**, *36*, 7–13.

(28) Bredikhin, A. A.; Zakharychev, D. V.; Fayzullin, R. R.; Antonovich, O. A.; Pashagin, A. V.; Bredikhina, Z. A. Chiral *para*-alkyl phenyl ethers of glycerol: synthesis and testing of chirality driven crystallization, liquid crystal, and gelating properties. *Tetrahedron: Asymmetry* **2013**, *24*, 807–816.

(29) Ernst, K.-H. On the validity of calling Wallach's rule Wallach's rule. *Israel J. Chem.* **2017**, *57*, 24-30.

(30) Brock, C. P.; Schweizer, W. B.; Dunitz, J. D. On the validity of Wallach rule: on the density and stability of racemic crystals compared with their chiral counterparts. *J. Amer. Chem. Soc*. **1991**, *113*, 9811–9820.

(31) Dunitz, J. D.; Gavezzotti, A. Proteogenic amino acids: chiral and racemic crystal packings and stabilities. *J. Phys. Chem. B*, **2012**, *116*, 6740–6750.

(32) Kennedy, A. R.; Morrison, C. A.; Briggs, N. E. B.; Arbuckle, W. Density and stability differences between enantiopure and racemic salts: construction and structural analysis of a systematic series of crystalline salt forms of methylephedrine. *Cryst. Growth Des.* **2011**, *11*, 1821–1834.

(33) Gavezzotti, A.; Rizzato, S. Are racemic crystals favored over homochiral crystals by higher stability or by kinetics? Insights from comparative studies of crystalline stereoisomers. *J. Org. Chem.* **2014**, *79*, 4809–4816.

(34) Lorenz, H.; Seidel-Morgenstern, A. Processes to separate enantiomers. *Angew. Chem. Int. Ed*. **2014**, *53*, 1218–1250.

(35) Levilain, G.; Coquerel, G. Pitfalls and rewards of preferential crystallization. *CrystEngComm* **2010**, *12*, 1983–1992.

For Table of Contents Use Only

Spontaneous resolution of chiral 3-(2,3-dimethylphenoxy)propane-1,2-diol under the circumstances of an unusual diversity of racemic crystalline modifications

Alexander A. Bredikhin, Dmitry V. Zakharychev, Zemfira A. Bredikhina, Alexey V. Kurenkov, Dmitry B. Krivolapov, Aidar T. Gubaidullin

Based on IR, X-ray diffraction and DSC data it was found that racemic 3-(2,3-dimethylphenoxy)propane-1,2-diol forms several crystalline modifications: four polymorphic racemic compounds and a racemic conglomerate. With the help of slurrying experiments, the nature of the transitions between solid phases was specified. Even a slight predominance of one of the enantiomers in almost racemic samples ensures the crystallization of the conglomerate.